

Adaptive Local Structure Consistency based Heterogeneous Remote Sensing Change Detection

Lin Lei, Yuli Sun, Gangyao Kuang, *Senior Member, IEEE*

Abstract—Change detection of heterogeneous remote sensing images is an important and challenging topic in remote sensing for emergency situation resulting from nature disaster. Due to the different imaging mechanisms of heterogeneous sensors, it is difficult to directly compare the images. To address this challenge, we explore an unsupervised change detection method based on adaptive local structure consistency (ALSC) between heterogeneous images in this letter, which constructs an adaptive graph representing the local structure for each patch in one image domain and then projects this graph to the other image domain to measure the change level. This local structure consistency exploits the fact that the heterogeneous images share the same structure information for the same ground object, which is imaging modality-invariant. To avoid the leakage of heterogeneous data, the pixelwise change image is calculated in the same image domain by graph projection. Experiment results demonstrate the effectiveness of the proposed ALSC based change detection method by comparing with some state-of-the-art methods.

Index Terms—Unsupervised change detection, Heterogeneous data, Adaptive local structure, Graph.

I. INTRODUCTION

Change detection (CD) is a process of identifying changes of an object or phenomenon by analyzing the remote sensing images acquired over the same geographical area at different times [1], [2]. Recently, heterogeneous CD has become a growing interest topic that allows the remote sensing community to make full use of the wide range of available earth observation satellites by considering the joint use of heterogeneous satellite images. In particular, the heterogeneous CD has important practical significance for the immediate evaluation of emergency disasters. In this case (such as earthquake or flood), the pre-event synthetic aperture radar (SAR) image is sometimes unavailable and the qualified post-event optical image cannot be obtained due to the adverse atmospheric conditions. Because different sensors provide different physical quantities for the same object and show different characteristics in the image, heterogeneous CD is a challenging task.

Heterogeneous CD is a challenging task since different sensors provide different physical quantities for the same object and show different characteristics in the images. Therefore, different from the algebraic methods (such as difference method, ratio method and log-ratio method) used in the homogeneous CD, it is impossible to compare the heterogeneous images directly to calculate the difference image (DI).

According to the different methods for generating the binary change map (CM), the existing heterogeneous CD methods can be roughly divided into three categories [3]: 1) classification-based methods, such as post-classification comparison (PC-C) [4], multitemporal segmentation and compound classification (MS-CC) [5], [6]; 2) deep-learning based methods, such as symmetric convolutional coupling network (SCCN) [7], logarithmic transformation feature learning (LTFL) based method [8], and conditional generative adversarial network (cGAN) [9]; 3) traditional DI-based methods, such as the local joint distributions with manifold learning based method [10], Markov model for multimodal change detection (M3CD) [11], supervised homogeneous pixel transformation (HPT) method [12], and affinity matrix based image regression (AM-IR) method [13]. The goal of the heterogeneous CD methods is to transform the “incomparable” heterogeneous images into a common “comparable” space, such as the category space of classification-based method, the learned high-dimensional feature space of deep learning-based method, and the constructed feature space of traditional DI-based method [3].

Recently, the self-similarity property is exploited to project the pre-event (post-event) image to the post-event (pre-event) image and then obtain a pixelwise DI for heterogeneous CD. In [14], the self-similarity property is used to complete the fractal projection, which contains a fractal encoding step and a fractal projection/decoding step. In [3], the self-similarity is used to complete self-expression, which learns a patch similarity graph matrix (PSGM) for each image and then measures the change level by multiplying one image with the learned PSGM from the other image and calculating the difference. In this letter, the self-similarity is further used to construct graphs representing the local structures for each image and establish the relationship between heterogeneous images, which is similar to the patch similarity graph based method in [15]. However, instead of using a fixed graph as [15], the proposed method adaptively learns a distance induced probabilistic graph, which is more robust. This local structure consistency exploits the fact that the heterogeneous images share the same structure information for the same ground object, which is imaging modality-invariant. Different from the previous fractal projection and PSGM based methods, the proposed ALSC based method neither reconstructs the image nor transforms the image to the domain of the other image. It only focuses on the changes of local structure. At the same time, it also takes into account the prior statistics of heterogeneous images that are not used in fractal projection [14] and PSGM [3], which makes the CD results more accurate. The main contributions of this letter are summarized

Manuscript received XX, XX. This work was partially supported by the National Natural Science Foundation of China (61971426). (*Corresponding author: Yuli Sun. Email: sunyuli@mail.ustc.edu.cn*)

L. Lei, Y. Sun and G. Kuang are with College of Electronic Science and Technology, National University of Defense Technology, Changsha 410073, China.

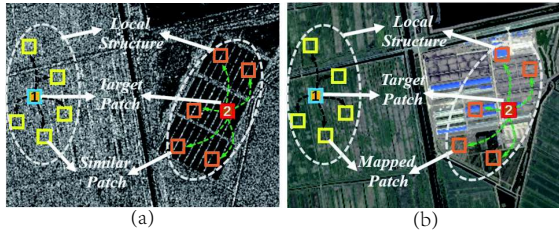


Fig. 1. Illustration of local structure consistency in heterogeneous images: (a) SAR image; (b) Optical image. The local structure of the unchanged target patch 1 in the SAR image can be preserved by the patch 1 in the optical image. However, for the changed target patch 2, the local structure in the SAR image is no longer conformed by the optical image.

as follows.

1) A heterogeneous CD method based on adaptive local structure consistency is proposed, which measures the change level between the pre- and post-event images by calculating how much the local structure of one image still conforms to that of the other image.

2) The leakage of heterogeneous data in the DI generation is avoided by the graph projection, which calculates the structure difference within the same image domain.

3) The ALS C based method is completely unsupervised, and it exploits the inherent structure property of any satellite image that appeals quite imaging modality-invariant, so it has a strong flexibility to deal with a variety of heterogeneous image processing tasks.

II. ALS C BASED HETEROGENEOUS CD METHOD

We consider two coregistered heterogeneous images, $\mathbf{X} = \{x(m, n, c) | 1 \leq m \leq M, 1 \leq n \leq N, 1 \leq c \leq C_{\mathbf{X}}\}$ lining in the domain \mathcal{X} and $\mathbf{Y} = \{y(m, n, c) | 1 \leq m \leq M, 1 \leq n \leq N, 1 \leq c \leq C_{\mathbf{Y}}\}$ lining in the domain \mathcal{Y} , which are acquired on the same geographical area by two different sensors at two different times, respectively. Here, M , N and $C_{\mathbf{X}}$ ($C_{\mathbf{Y}}$) represents the height, width and channel number of two images, respectively.

Using the self-similarity property, a small patch in the image can always find some similar patches within the image. This relationship between the target patch and its similar patches (K -nearest neighbors) can be regarded as the local structure of this target patch, which is quite well preserved across the different types of imaging modality [15]. As shown in Fig. 1, in the SAR image \mathbf{X} , the local structure of target patch \mathbf{X}_i is represented by the relationship between \mathbf{X}_i and its similar patches \mathbf{X}_j . If the area represented by these patches has not changed in the event, the local structure of target patch \mathbf{X}_i can be preserved by the patch \mathbf{Y}_i in the optical image \mathbf{Y} , which means that the patch \mathbf{Y}_i is also very similar to the patches \mathbf{Y}_j . On the contrary, if the area represented by \mathbf{X}_i has changed in the event, the local structure is no longer preserved by \mathbf{Y}_i , showing that \mathbf{Y}_i and \mathbf{Y}_j are very different. Therefore, we can see that the ALS C based heterogeneous CD method mainly needs to solve two problems: how to construct local structure and how to measure structural difference. The proposed method consists of four steps: 1) construct adaptive

local structure; 2) calculate the structure difference; 3) generate the difference image; 4) obtain the binary change map.

A. Adaptive local structure

For a square target patch, $\mathbf{X}_i = \{x(m_i + \vartheta_m, n_i + \vartheta_n, c) | \vartheta_m, \vartheta_n \in [-p, p], 1 \leq c \leq C_{\mathbf{X}}\} \in \mathbb{R}^{(2p+1) \times (2p+1) \times C_{\mathbf{X}}}$ centered on position (m_i, n_i) , in order to capture the local structure of \mathbf{X}_i , we construct a graph by adaptively assigning a probability $S_{i,j}^{\mathbf{X}}$ for \mathbf{X}_j as the neighborhood of \mathbf{X}_i , and the probability is treated as the similarity between two patches, where \mathbf{X}_j is another patch in a $\omega \times \omega$ search window \mathbb{W} centered on (m_i, n_i) . Here, we use a search step size $\Delta_s > 1$ in \mathbb{W} to make the distance between adjacent patches equal to Δ_s , which can reduce the number of neighbors and avoid redundancy.

Usually, a smaller distance between \mathbf{X}_i and \mathbf{X}_j should be assigned a large probability $S_{i,j}^{\mathbf{X}}$. To achieve this goal, we can solve the following problem

$$\min_{S_{i,j}^{\mathbf{X}}} \sum_{j=1}^{N_s} dist_{i,j}^{\mathbf{X}} S_{i,j}^{\mathbf{X}} + \gamma (S_{i,j}^{\mathbf{X}})^2 \text{ s.t. } 0 \leq S_{i,j}^{\mathbf{X}} \leq 1, \sum_{j=1}^{N_s} S_{i,j}^{\mathbf{X}} = 1 \quad (1)$$

where $dist_{i,j}^{\mathbf{X}}$ represents a distance measure of two patches \mathbf{X}_i and \mathbf{X}_j , N_s is the the number of all potential neighbors of \mathbf{X}_i in the search window \mathbb{W} , and $\gamma > 0$ is the trade-off parameter. The second term of the objective function in (1) is a regularization, which is used to avoid the trivial solution, i.e., only the nearest patch can be the neighbor of \mathbf{X}_i with probability 1 (when $\gamma = 0$). If we only focus on the second term (when $\gamma \rightarrow \infty$), the optimal solution of (1) is that all the patches in \mathbb{W} can be the neighbors of \mathbf{X}_i with the same probability $1/N_s$.

The patch distance $dist_{i,j}^{\mathbf{X}}$ should be computed based on the prior statistics of the image \mathbf{X} . For two patches \mathbf{X}_i and \mathbf{X}_j , we vectorized them and denote each element as $x_i(q)$ and $x_j(q)$ with $x_j(q)$, respectively. 1) For the optical image, assuming the additive white Gaussian noise (AWGN) model, the traditional Euclidean distance is usually used

$$dist_{i,j}^{\mathbf{X}} = \|\mathbf{X}_i - \mathbf{X}_j\|_F^2 \quad (2)$$

2) For the SAR image, assuming the multiplicative speckle noise modeled by a Gamma distribution, the following distance criterion [16] can be used

$$dist_{i,j}^{\mathbf{X}} = \sum_{q=1}^{(2p+1)^2 C_{\mathbf{X}}} \log \left(\frac{x_i(q) + x_j(q)}{2\sqrt{x_i(q)x_j(q)}} \right) \quad (3)$$

It should be noted that the distance calculation function is not fixed, which should be determined according to the prior statistical information of the image.

Denote $S_i^{\mathbf{X}} \in \mathbb{R}^{N_s}$ and $dist_i^{\mathbf{X}} \in \mathbb{R}^{N_s}$ as column vectors composed of $S_{i,j}^{\mathbf{X}}$ and $dist_{i,j}^{\mathbf{X}}$, respectively, and denote $\mathbf{1}$ as a column vector with all the elements being one, the problem (1) can be reformulated as

$$\min_{(S_i^{\mathbf{X}})^T \mathbf{1} = 1, 0 \leq S_{i,j}^{\mathbf{X}} \leq 1} \left\| S_i^{\mathbf{X}} - \frac{1}{2\gamma} dist_i^{\mathbf{X}} \right\|_2^2 \quad (4)$$

TABLE I
IMPLEMENTATION STEPS OF ALGORITHM 1.

Algorithm 1. The optimization algorithm of minimization (4)
Input: Distance vector $dist_i^{\mathcal{X}}$ and the number of nearest neighbors K .
1. Sorting $dist_i^{\mathcal{X}}$ in ascending order as $dist_{i,i_{\mathbf{X}}^{(1)}}^{\mathcal{X}}, \dots, dist_{i,i_{\mathbf{X}}^{(N_s)}}^{\mathcal{X}}$.
2. Calculating the $S_i^{\mathbf{X}}$ with
$S_{i,i_{\mathbf{X}}^{(h)}}^{\mathbf{X}} = \begin{cases} \frac{dist_{i,i_{\mathbf{X}}^{(K+1)}}^{\mathcal{X}} - dist_{i,i_{\mathbf{X}}^{(h)}}^{\mathcal{X}}}{K dist_{i,i_{\mathbf{X}}^{(K+1)}}^{\mathcal{X}} - \sum_{r=1}^K dist_{i,i_{\mathbf{X}}^{(r)}}^{\mathcal{X}}}, & h \leq K \\ 0, & h > K \end{cases}$
Output: The similarity vector $S_i^{\mathbf{X}}$.

This problem naturally has a sparse solution, which means that the target patch \mathbf{X}_i is only connected with its K -nearest neighbors (K-NN). That is, we just to learn $S_i^{\mathbf{X}}$ with K nonzero entries. This problem can be solved with a closed solution as in [17]. By denoting $dist_{i,i_{\mathbf{X}}^{(h)}}^{\mathcal{X}}$ with $h = 1, 2, \dots, N_s$ as the h -th smallest element of $dist_i^{\mathcal{X}}$, we give a summary of this efficient solution as shown in Algorithm 1 of Table I, and more details can be found in [17].

From Algorithm 1, we can find that the regularization parameter γ is replaced by the number of neighbors K , which are equivalent when we set γ to be

$$\gamma = \frac{K}{2} dist_{i,i_{\mathbf{X}}^{(K+1)}}^{\mathcal{X}} - \frac{1}{2} \sum_{r=1}^K dist_{i,i_{\mathbf{X}}^{(r)}}^{\mathcal{X}} \quad (5)$$

In this way, the search of parameter γ can be better handled by searching the neighborhood size K , which is more intuitive (it has explicit meaning) and easy to tune (it is an integer).

B. Calculate the structure difference

As the local structure of patches \mathbf{X}_i and \mathbf{Y}_i can be represented by $S_i^{\mathbf{X}}$ and $S_i^{\mathbf{Y}}$, we need to compare them to calculate the structure difference. However, because $S_i^{\mathbf{X}}$ and $S_i^{\mathbf{Y}}$ are generated based on different distance vectors $dist_i^{\mathcal{X}}$ and $dist_i^{\mathcal{Y}}$, which are calculated on different domains \mathcal{X} and \mathcal{Y} , directly comparing $S_i^{\mathbf{X}}$ and $S_i^{\mathbf{Y}}$ (such as $\|S_i^{\mathbf{X}} - S_i^{\mathbf{Y}}\|_2$) will cause the leakage of heterogeneous data. To avoid the leakage, we first project the graph $S_i^{\mathbf{X}}$ (or $S_i^{\mathbf{Y}}$) of image domain \mathcal{X} (or \mathcal{Y}) to the other image domain \mathcal{Y} (or \mathcal{X}), and then compare the difference in the same image domain to obtain the structure difference. Therefore, we can compute the forward structure difference $f_i^{\mathbf{Y}}$ and the backward structure difference $f_i^{\mathbf{X}}$ as

$$f_i^{\mathbf{Y}} = \sum_{h=1}^{h=K} dist_{i_{\mathbf{Y}}^{(h)}, i_{\mathbf{X}}^{(h)}}^{\mathcal{Y}} S_{i,i_{\mathbf{X}}^{(h)}}^{\mathbf{X}}, \quad f_i^{\mathbf{X}} = \sum_{h=1}^{h=K} dist_{i_{\mathbf{Y}}^{(h)}, i_{\mathbf{X}}^{(h)}}^{\mathcal{X}} S_{i,i_{\mathbf{Y}}^{(h)}}^{\mathbf{Y}} \quad (6)$$

The intuitive explanation of $f_i^{\mathbf{Y}}$ in (6) is: for the patch \mathbf{X}_j with $j = i_{\mathbf{X}}^{(h)}$, which is the h -th nearest neighbor of target patch \mathbf{X}_i , the $dist_{i_{\mathbf{Y}}^{(h)}, i_{\mathbf{X}}^{(h)}}^{\mathcal{Y}}$ is the patch difference between the projected patch \mathbf{Y}_j (that is $\mathbf{Y}_{i_{\mathbf{X}}^{(h)}}$) and the h -th nearest neighbor of patch \mathbf{Y}_i (that is $\mathbf{Y}_{i_{\mathbf{Y}}^{(h)}}$), and the $S_{i,i_{\mathbf{X}}^{(h)}}^{\mathbf{X}}$ is the weight of this patch difference. From this, we can find that the patch difference is calculated in the same image domain, which avoids the leakage of heterogeneous data.

TABLE II
IMPLEMENTATION STEPS OF GENERATING THE ALSC BASED DI.

Algorithm 2. ALSC based DI generation
Input: Heterogeneous images \mathbf{X}, \mathbf{Y} , parameters $p, \omega, \Delta_p, \Delta_s$ and K .
1. Calculate the structure difference
for all target patches $\mathbf{X}_i, \mathbf{Y}_i, i \in \Lambda$ do
Compute the distances $dist_i^{\mathcal{X}}$ and $dist_i^{\mathcal{Y}}$ with different criteria.
Compute the similarities $S_i^{\mathbf{X}}$ and $S_i^{\mathbf{Y}}$ by using Algorithm 1.
Compute the structure difference $f_i^{\mathbf{X}}$ and $f_i^{\mathbf{Y}}$.
Add $f_i^{\mathbf{X}}$ and $f_i^{\mathbf{Y}}$ to the sets $F_j^{\mathbf{X}}$ and $F_j^{\mathbf{Y}}$, respectively.
end for
2. Compute the forward and backward DIs
for all pixels $j, j = 1, \dots, MN$ do
Compute the forward $DI^{\mathbf{Y}}$ and backward $DI^{\mathbf{X}}$.
end for
3. Fuse the forward and backward DIs
$DI^{final} = DI^{\mathbf{X}} / \text{mean}(DI^{\mathbf{X}}) + DI^{\mathbf{Y}} / \text{mean}(DI^{\mathbf{Y}})$

C. Generate the difference image

Once the forward structure difference $f_i^{\mathbf{Y}}$ is calculated, it is assigned to all the pixels of patch \mathbf{Y}_i . After we calculate the forward structure differences for all the overlapping patches of the two images, for each pixel $j, j = 1, \dots, MN$ in the forward DI there is a set $F_j^{\mathbf{Y}}$ of structure difference that covers the pixel j . Therefore, the final forward change level of this specific pixel j is the mean of this set as

$$DI_j^{\mathbf{Y}} = \frac{1}{|F_j^{\mathbf{Y}}|} \sum_{f_i^{\mathbf{Y}} \in F_j^{\mathbf{Y}}} f_i^{\mathbf{Y}} \quad (7)$$

Then we can obtain the forward difference image $DI^{\mathbf{Y}}$. At the same time, the backward $DI^{\mathbf{X}}$ can also be generated in a similar way. We can obtain the final DI^{final} by fusing the forward $DI^{\mathbf{Y}}$ and backward $DI^{\mathbf{X}}$ as

$$DI^{final} = DI^{\mathbf{X}} / \text{mean}(DI^{\mathbf{X}}) + DI^{\mathbf{Y}} / \text{mean}(DI^{\mathbf{Y}}) \quad (8)$$

Given the set Λ of all target patches spaced by a patch step size $\Delta_p \in [1, p)$, Algorithm 2 listed in Table II summarizes the procedure of generating the ALSC based DI. With this Δ_p , the amount of target patches can be reduced by a factor of Δ_p^2 , thereby speeding up the algorithm.

D. Obtain the binary change map

After the fused DI is obtained, the CD can be completed as an binary segmentation problem. Then, we can use the thresholding method (such as the Otsu threshold method [18]) or the clustering method (such as the PCAKM [19] that using principal component analysis to extract the features and employing the k -means with $k = 2$) to obtain the binary CM.

III. EXPERIMENTAL RESULTS

A. Data description

Four pairs of heterogeneous data sets are selected to assess the effectiveness of the proposed ALSC based heterogeneous CD method, as shown in Figs. 2(a)-(c).

(1) Sardinia data set: a pair of near-infrared (NIR) band/optical images. The $300 \times 412 \times 1$ NIR image is acquired by Landsat-5 and the $300 \times 412 \times 3$ optical image is obtained from Google Earth. The ground truth shows the expansion of

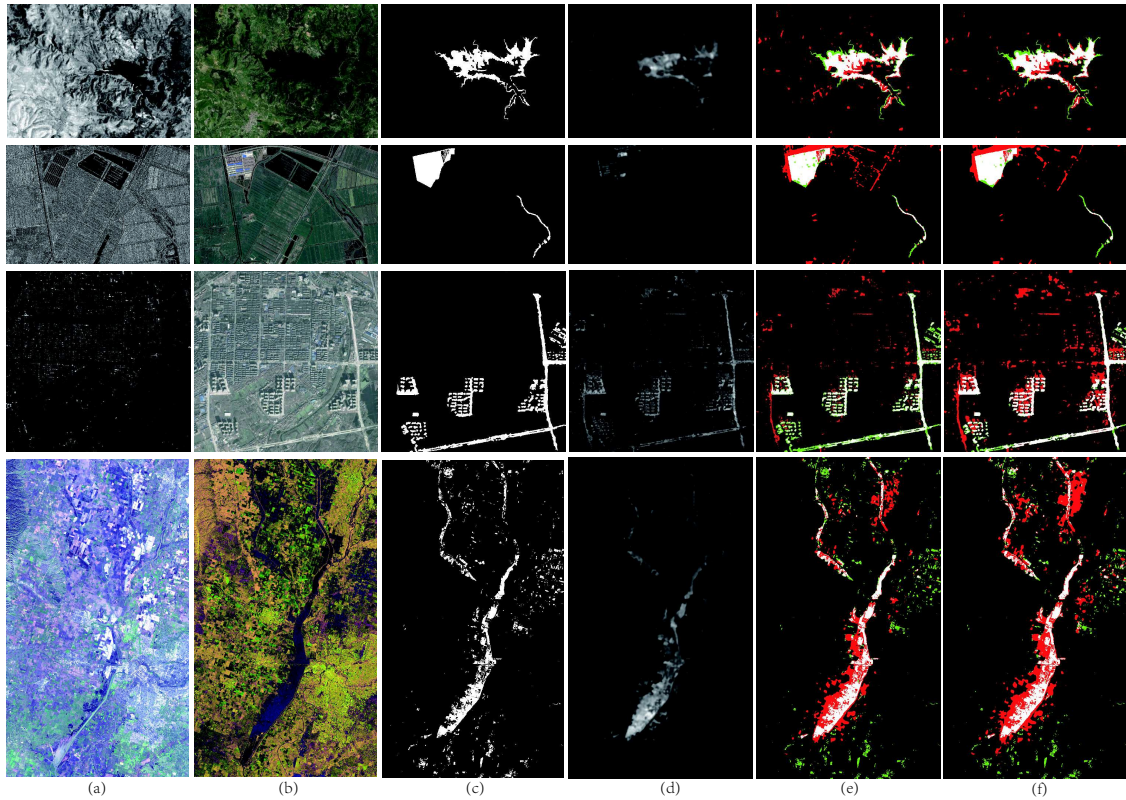


Fig. 2. ALSC based DI and binary CM on different data sets. From top to bottom, they correspond to Sardinia, Shuguang, Wuhan and California data sets, respectively. From left to right are: (a) pre-event image; (b) post-event image; (c) the ground truth image; (d) ALSC based DI; (e) binary CM of ALSC-O; (f) binary CM of ALSC-P. In the binary CM, White: true positives (TP); Red: false positives (FP); Black: true negatives (TN); Green: false negatives (FN).

Lake Mulargia, on the island of Sardinia, Italy. (2) Shuguang data set: a pair of SAR/optical images. The $593 \times 921 \times 1$ SAR image is acquired by Radarsat-2 and the $593 \times 921 \times 3$ optical image is obtained from Google Earth. The ground truth shows the changes of land use in Shuguang Village, Dongying City, China. (3) Wuhan data set: a pair of SAR/optical images. The $495 \times 503 \times 1$ SAR image is acquired by Radarsat-2 and the $495 \times 503 \times 3$ optical image is obtained from Google Earth. The ground truth shows the changes of new buildings and roads in Wuhan City, China. (4) California data set: a pair of multispectral/SAR images. The $875 \times 500 \times 11$ multispectral image is acquired by Landsat-8 and the $875 \times 500 \times 3$ SAR image is acquired by Sentinel-1A, which is recorded in polarisations VV and VH, and augmented with the ratio between the two intensities as the third channel. The ground truth shows a flood in California, USA, which is provided by Luppino et al. [13].

B. Experimental results and analysis

As listed in Table II, the parameters of ALSC based method are the patch size p , the search window size ω , the patch step size Δ_p , the search step size Δ_s , and the number of neighbors K . For all the experimental results, we fix $\omega = 75p$, $\Delta_p = p$, $\Delta_s = 2p + 1$, $K = 35$, and vary the p from 1 to 4 to select the best one for each data set. Specifically, we set $p = 1$ for Wuhan, $p = 2$ for Sardinia and California, and $p = 3$ for Shuguang.

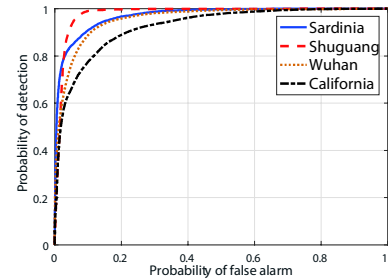


Fig. 3. ROC curves of ALSC generated DI.

Fig. 2(d) shows the ALSC generated DI of different data sets. We can find that the proposed ALSC can well establish the relationship between heterogeneous images, which can highlight the changes in the DI. Fig. 3 plots the empirical receiver operating characteristics (ROC) curves of ALSC generated DI, and shows that the quality of these DI is very high, which gain a large area under the ROC curves as 0.970, 0.979, 0.957 and 0.925 for Sardinia, Shuguang, Wuhan and California data sets, respectively.

With these ALSC based DI, the binary CM can be obtained by using the Otsu thresholding (denoted as ALSC-O for short) and PCAKM (denoted as ALSC-P for short), as shown in Figs. 2(e)-(f). Four measures are considered as the evaluation criteria of CM: the false positives (FP) rate, the false negatives (FN) rate, the overall accuracy (OA), and the Kappa coefficient

TABLE III
QUANTITATIVE MEASURES OF ALSC BASED BINARY CM.

Data sets	ALSC-O			ALSC-P		
	FP(%)	FN(%)	KC	FP(%)	FN(%)	KC
Sardinia	2.42	1.35	0.6983	2.10	1.40	0.7134
Shuguang	3.65	0.52	0.6410	3.11	0.55	0.6693
Wuhan	1.76	2.83	0.5950	5.82	1.01	0.5849
California	4.07	1.57	0.4697	6.05	1.31	0.4201

TABLE IV
ACCURACY RATE OF CM GENERATED BY THE PROPOSED METHOD AND SOME SOTA COMPARISON METHODS ON DIFFERENT DATA SETS (WITH THE OPTIMAL TWO VALUES WRITTEN IN BOLD FOR EACH DATA SET).

Sardinia	OA	Shuguang	OA	Wuhan	OA	California	OA
ALSC-O	0.962	ALSC-O	0.958	ALSC-O	0.954	ALSC-O	0.944
ALSC-P	0.965	ALSC-P	0.963	ALSC-P	0.932	ALSC-P	0.926
FP-MS ^[14]	0.928	FP-MS ^[14]	0.942	LTFL ^[8]	0.952	FP-MS ^[14]	0.952
PSGM ^[3]	0.961	PSGM ^[3]	0.977	PSGM ^[3]	0.953	AM-IR ^[13]	0.933
M3CD ^[11]	0.964	NPSG ^[15]	0.975	NPSG ^[15]	0.958	NPSG ^[15]	0.941
RMN ^[20]	0.847	RMN ^[20]	0.884				
AFL-DSR ^[21]	0.929	AFL-DSR ^[21]	0.980				

(KC). Table III reports the quantitative measures of ALSC based binary CM of different heterogeneous data sets. From Figs. 2(e)-(f) and Table III, we can see that the changed and unchanged area are well detected with relatively small FN and FP.

In order to further evaluate the performance of ALSC, some representative and state-of-the-art (SOTA) methods including PSGM [3], LTFL [8], M3CD [11], AM-IR [13], fractal projection and Markovian segmentation-based method (FP-MS) [14], nonlocal patch similarity graph-based method (NPSG) [15], reliable mixed-norm-based heterogeneous CD method (RMN) [20], and anomaly feature learning based deep sparse residual model (AFL-DSR) [21], are selected for comparison as summarized in Table IV. We can see that ALSC can achieve better or quite competitive performance by comparing with these SOTA methods, and ALSC shows the ability to gain consistent good results on different data sets. The average accuracy rates obtained on four heterogeneous data set of the ALSC with Otsu thresholding and PCAKM are 95.46% and 94.66%, respectively.

IV. CONCLUSION

In this letter, we mainly address the problem of change detection in heterogeneous remote sensing. To find out a relationship between heterogeneous images and make them comparable, we explore the ALSC between heterogeneous images, which exploits the inherent structure property of images and appeals quite imaging modality-invariant. The core idea of the ALSC is that the local structure of each target patch in the pre-event (post-event) image will keep invariance in the post-event (pre-event) image when there is no change occurred; on the contrary, once a change occurred within this target patch, this local invariance will no longer be maintained. Therefore, the ALSC based CD method can be implemented in two steps. It first constructs adaptive local structure for each input image, and then compare the structure difference in the same image domain by graph projection, which can avoid the leakage of heterogeneous data. Experimental results clearly show that the ALSC based CD method can achieves effective performance on different heterogeneous data sets.

REFERENCES

- [1] A. SINGH, "Review article digital change detection techniques using remotely-sensed data," *Int. J. Remote Sens.*, vol. 10, no. 6, pp. 989-1003, Jun. 1989.
- [2] F. Bovolo and L. Bruzzone, "The time variable in data fusion: a change detection perspective," *IEEE Geosci. Remote Sens. Mag.*, vol. 3, no. 3, pp. 8-26, Sept. 2015.
- [3] Y. Sun, L. Lei, X. Li, X. Tan, and G. Kuang, "Patch similarity graph matrix based unsupervised remote sensing change detection with homogeneous and heterogeneous sensors," *IEEE Trans. Geosci. Remote Sens.*, Early Access, 2020, doi: 10.1109/TGRS.2020.3013673.
- [4] W. Zhou, A. Troy, and M. Grove, "Object-based land cover classification and change analysis in the baltimore metropolitan area using multitemporal high resolution remote sensing data," *Sensors*, vol. 8, no. 3, pp. 1613-1636, Mar. 2008.
- [5] L. Wan, Y. Xiang, and H. You, "A post-classification comparison method for SAR and optical images change detection," *IEEE Geosci. Remote Sens. Lett.*, vol. 16, no. 7, pp. 1026-1030, Jul. 2019.
- [6] L. Wan, Y. Xiang, and H. You, "An object-based hierarchical compound classification method for change detection in heterogeneous optical and SAR images," *IEEE Trans. Geosci. Remote Sens.*, vol. 57, no. 12, pp. 9941-9959, Dec. 2019.
- [7] J. Liu, M. Gong, K. Qin, and P. Zhang, "A deep convolutional coupling network for change detection based on heterogeneous optical and radar images," *IEEE Trans. Neural Netw. Learn. Syst.*, vol. 29, no. 3, pp. 545-559, Mar. 2018.
- [8] T. Zhan, M. Gong, X. Jiang, and S. Li, "Log-based transformation feature learning for change detection in heterogeneous Images," *IEEE Geosci. Remote Sens. Lett.*, vol. 15, no. 9, pp. 1352-1356, Sep. 2018.
- [9] X. Niu, M. Gong, T. Zhan, and Y. Yang, "A conditional adversarial network for change detection in heterogeneous images," *IEEE Geosci. Remote Sens. Lett.*, vol. 16, no. 1, pp. 45-49, Jan. 2019.
- [10] J. Prendes, M. Chabert, F. Pascal, A. Giros, and J.-Y. Tourneret, "A new multivariate statistical model for change detection in images acquired by homogeneous and heterogeneous sensors," *IEEE Trans. Image Process.*, vol. 24, no. 3, pp. 799-812, Mar. 2015.
- [11] R. Touati, M. Mignotte, and M. Dahmane, "Multimodal change detection in remote sensing images using an unsupervised pixel pairwise based Markov random field model," *IEEE Trans. Image Process.*, vol. 29, pp. 757-767, Aug. 2019.
- [12] Z. Liu, G. Li, G. Mercier, Y. He, and Q. Pan, "Change detection in heterogeneous remote sensing images via homogeneous pixel transformation," *IEEE Trans. Image Process.*, vol. 27, no. 4, pp. 1822-1834, Apr. 2018.
- [13] L. T. Luppino, F. M. Bianchi, G. Moser, and S. N. Anfinsen, "Unsupervised image regression for heterogeneous change detection," *IEEE Trans. Geosci. Remote Sens.*, vol. 57, no. 12, pp. 9960-9975, Dec. 2019.
- [14] M. Mignotte, "A fractal projection and Markovian segmentation-based approach for multimodal change detection," *IEEE Trans. Geosci. Remote Sens.*, Early Access, 2020, doi: 10.1109/TGRS.2020.2986239.
- [15] Y. Sun, L. Lei, X. Li, H. Sun, and G. Kuang, "Nonlocal patch similarity based heterogeneous remote sensing change detection," *Pattern Recognit.* vol. 109, pp. 107598, Jan. 2021.
- [16] C.-A. Deledalle, L. Denis, and F. Tupin, "How to compare noisy patches? Patch similarity beyond Gaussian noise," *Int. J. Comput. Vis.*, vol. 99, no. 1, pp. 86-102, Aug. 2012.
- [17] F. Nie, X. Wang, and H. Huang, "Clustering and projected clustering with adaptive neighbors," in *Proc. ACM SIGKDD*, Aug. 2014, pp. 977-986.
- [18] N. Otsu, "A threshold selection method from gray-Level histograms," *IEEE Trans. Syst. Man Cybern. -Syst.*, vol. 9, no. 1, pp. 62-66, Jan. 1979.
- [19] Turgay Celik, "Unsupervised change detection in satellite images using principal component analysis and k-means clustering," *IEEE Geosci. Remote Sens. Lett.*, vol. 6, no. 4, pp. 772-776, Oct. 2009.
- [20] R. Touati, M. Mignotte, and M. Dahmane, "A reliable mixed-norm-based multiresolution change detector in heterogeneous remote sensing images," *IEEE J. Sel. Top. Appl. Earth Observ. Remote Sens.*, vol. 12, no. 9, pp. 3588-3601, Sept. 2019.
- [21] R. Touati, M. Mignotte, and M. Dahmane, "Anomaly feature learning for unsupervised change detection in heterogeneous images: a deep sparse residual model," *IEEE J. Sel. Top. Appl. Earth Observ. Remote Sens.*, vol. 13, pp. 588-600, 2020.